EXPERIMENTAL STUDY ON SEISMIC BEHAVIOR OF REINFORCED CONCRETE CORE WALL

DU Xiu-li[1], JIA Peng[2] And ZHAO Jun[3]
[1]*Professor, College of Architecture and Civil Engineering, Beijing University of Technology, Beijing, China*
[2]*Doctor, College of Architecture and Civil Engineering, Beijing University of Technology, Beijing, China*
[3]*Professor, College of Architecture and Civil Engineering, Beijing University of Technology, Beijing, China*
Email: jiapeng@emails.bjut.edu.cn, duxl@iwhr.com

ABSTRACT:
In order to further study the seismic behavior and influencing factors of reinforced concrete core wall, three reinforced concrete core wall models with large height-width ratio were built and tested to failure under the combined action of constant axial load and reversed cyclic lateral load. The axial compression ratio and span-depth ratio of coupling beam of each core wall were focused on. This paper presents the results, including failure mode, hysteretic behavior, load-carrying capacity, ductility, energy dissipation ability, shear lag effect. The final overall bending damage occurred at the bottom of each model. When the axial compression ratio increasing or span-depth ratio of coupling beam dropping, stiffness and load-carrying capacity of the specimen had risen markedly, but the ductility performance dropped significantly. It can be concluded from the analysis that the axial compression ratio and span-depth ratio of coupling beam both have important effects on the seismic behavior of reinforced concrete core wall.

KEYWORDA: axial compression, coupling beam, load testing, seismic behavior, reinforced concrete core wall

1. INTRODUCTION

Recently, many high-rise RC structures with reinforced concrete core wall have been designed and constructed in China. Reinforced concrete core wall which has large horizontal stiffness and load carrying capacities is the key component when the RC structure subjected to earthquake. When a high-rise RC structure with reinforced concrete core wall is designed in a seismic area, it is important to evaluate the structural capacities of the structure, especially reinforced concrete core wall subjected to lateral load.

As for huge structure in reality, even specimen with a scale model is still very tall; therefore, subjected to conditions of test, only a smaller size section and smaller height specimens can be tested in laboratory. In addition, the high axial compression ratios of the actual structure in experiments are difficult to simulate. Among the specimens tested at home and abroad, the height-width ratio and axial compression ratio of reinforced concrete core wall are generally low, which are significantly different from the actual. In order to reflect the structural capacities of the real reinforced concrete core wall as far as possible, specimens with larger height-width ratio and axial compression ratio should be tested and studied. Beijing University of Technology recently carried out work in this area.

This project was aimed at the investigation of the seismic behavior of the reinforced concrete core wall through a combined experimental and analytical research program. According to the existing conditions of lab, three reinforced concrete core wall models with large height-width ratio were built and tested to failure under the combined action of constant axial load and reversed cyclic lateral load. Seismic behavior of reinforced concrete core wall under different axial compression ratio and span-depth ratio of coupling beam was focused on.

2. STRUCTURAL TEST

2.1. Specimens and Test Method

Fig.1 shows the test reinforced concrete core wall consisting of four shear walls and 6-stories with 0.615m story height. Total height of test building was 3.69m. The model scale was 1:6.5 and the height-width ratio of specimen was 2.68. Three specimens were tested. All specimens had the same size and reinforcement, except TC3 having different size of coupling beams. Fig.1 shows the details of the specimens and rebar arrangement. X-shaped rebar arrangement was applied to coupling beams.The maximum size of concrete coarse aggregate was 10mm diameter, and the compressive strength measured was 26N/mm^2 at the time of test.

Experimental parameters were axial compression ratio and span-depth ratio of coupling beam. The axial compression ratios were 0.21 for TC1, 0.5 for TC2, and 0.21 for TC3. The span-depth ratios of coupling beam were varied: 1.7, 1.7 and 0.9.

In each test, the vertical load was imposed on the top of the specimen firstly and remained unchanged during the whole test. Reversed cyclic lateral load was imposed on the top and third story of the specimen and these two loads were varied according to inverted triangle. In the process of loading, the lateral load was under combined control of force and displacement. During first to third loading level, the lateral load was controlled by force and thereafter was controlled by displacement. When the load dropped by approximately 15% of the maximum load, test ended.

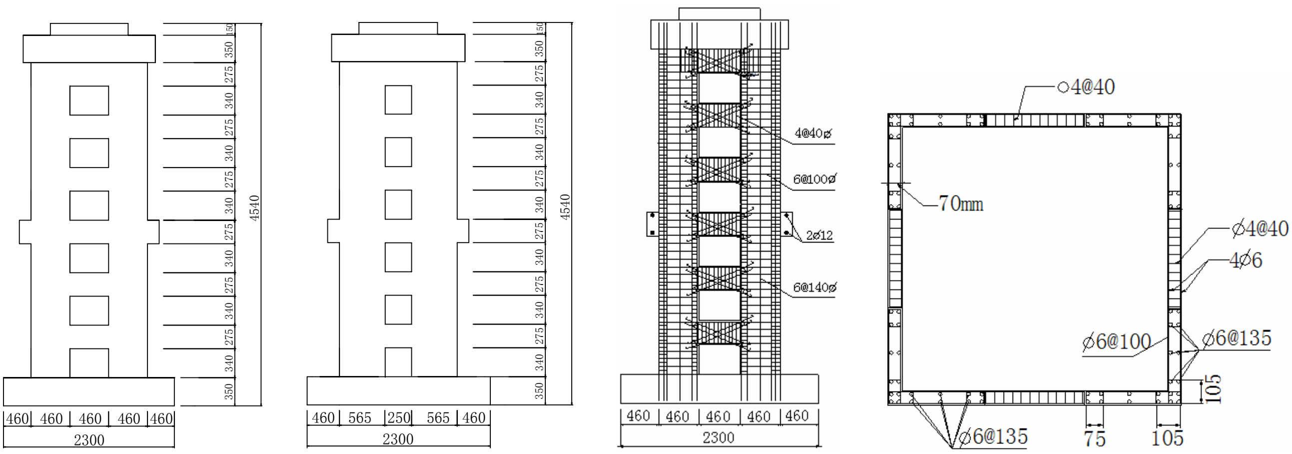

Fig 1 Dimensions of the core-wall and Position of Reinforcement of TC1 and TC2

3. TEST RESULTS

3.1. Cracking and crushing of reinforced concrete core wall

TC1 specimen

During first level of loading, there were no cracks and specimen was in elastic stage. During second level of loading, first vertical cracks occurred in one end of coupling beam of second story and then in the same places of coupling beams of third to fifth story vertical cracks initiated. Soon a crack orienting at approximately 45^0 to a horizontal line initiated in the middle of coupling beam of second story. All cracks closed after unloading. During third level of loading, first horizontal bending crack occurred in the bottom of flange wall and then a few horizontal cracks initiated from the bottom to up in the flange wall. A few oblique shear cracks occurred in web wall. Those horizontal and oblique cracks trended to intersect at the corners of specimen.

When the top horizontal displacement D=20mm, cracks in the ends of the coupling beam turned to through-racks. Horizontal bending cracks in flange walls opened to a width of 0.3mm and progressed from the bottom to up. Many new oblique shear cracks occurred in web walls. When D=28mm, the width of crack opening in the ends of the coupling beam reached 2mm and oblique cracks progressed. Spalling of concrete occurred at the bottom corner of web wall and flange wall. When D=36mm, a vertical crack in the end of the coupling beam opened to a width of 4mm and oblique cracks in coupling beams turned to X-shape. Width of horizontal crack opening in the bottom of flange wall reached 3mm and width of oblique crack opening in web wall reached 2mm. More of the concrete spalled around cracks in web wall and flange wall. When D=44mm, width of horizontal crack opening in the flange wall of first floor reached 5mm and width of oblique crack opening in web wall reached 5mm. When D=56mm, concrete in the bottom of flange wall was severely crushed and the specimen was in overall bending damage.


Fig 2 Distribution of cracks on web and final overall bending damage of TC1

TC2 specimen

During first to second level of loading, TC2 had the same phenomena with TC1. During third level of loading, cracks in the ends of second and third story turned to through-racks, but wall limb of specimen was intact and no cracks occurred.

When the top horizontal displacement D=12.6mm, horizontal cracks appeared in the bottom of flange wall and a few oblique cracks occurred in web wall. When D=16.8mm, the width of crack opening in the ends of the coupling beam reached 1.5mm and oblique cracks turned to X-shape. Horizontal bending cracks in flange wall had come to the second floor. When D=28.8mm, a vertical crack in the end of the coupling beam opened to a width of 4mm. Oblique cracks in web wall of lower story turned to several X-shape. Horizontal cracks in flange wall came to the third floor. When D=36.8mm, spalling of concrete occurred in couple beams of second and third story and in the bottom corner of specimen in compression. When D=40.8mm, more of the concrete spalled severely in the bottom corner of specimen. When D=44.8mm, concrete in the bottom of flange wall was severely crushed, test ended and specimen was in overall bending damage in final.

Fig 3 Distribution of cracks on web and final overall bending damage of TC2

TC3 specimen

During first to second level of loading, TC2 had the same phenomena with TC1 and TC2. During third level of loading, first horizontal bending crack occurred in the bottom of flange wall and a few oblique shear cracks occurred in web wall. New vertical and oblique cracks occurred in coupling beams.

When the top horizontal displacement D=16.8mm, widths of crack openings in coupling beams of first to third story increased. A lot of horizontal bending cracks initiated in flange walls from first to third story and many oblique shear cracks initiated in web walls in the bottom and those cracks turned to intersect at the corners of specimen. When D=28mm, spalling of concrete occurred around cracks in coupling beams of second and third story and in the bottom of flange wall and a long horizontal crack occurred at intersection of web wall and foundation. When D=40mm, no more new cracks formed in coupling beams but the widths of crack openings in the ends of coupling beams continued to increase. Widths of oblique shear cracks in web walls increased evidently and trended to intersect through coupling beams.Widths of horizontal fractures in the bottom of flange walls in tension continued to increase. When D=40mm, widths of horizontal fractures in the bottom of flange walls in tension reached 4mm, concrete in the bottom of flange walls in compression was crushed and test ended.

Fig 4 Distribution of cracks on web and final overall bending damage of TC3

3.2. Hysteretic behavior

Before specimens cracking, loading curves and unloading curves were almost coincident, hysteretic curves were similar to linear and areas of hysteretic loops were small showing specimens in elastic stage. During cracking beginning, minor cracking occurred at the two ends of coupling beam and the bottom of the core wall, stiffness of specimens were declined and hysteretic loops were spindle. As cracking occurring and progressing continuously, hysteretic curves began to show “pinch shrinkage” phenomenon and hysteretic loops trended to bow shape, which reflecting the effect of certain steels sliding. Areas of hysteretic loops gradually increased, indicating stable energy dissipation capacity. During the end of loading, hysteretic loop of TC1 trended to reverse S shape, as for the plastic hinges at the bottom of core wall and the two ends of coupling beams rotating fully and width of cracks increasing gradually. Because larger axial force restraining crack opening, hysteretic curve of TC2 was steep and had little trend to reverse S shape. Hysteretic loop of TC3 kept bow shape and showed “pinch shrinkage” evidently, due to larger relative stiffness of coupling beams restraining the plastic hinges at the ends of coupling beams rotating and crack opening in coupling beams.

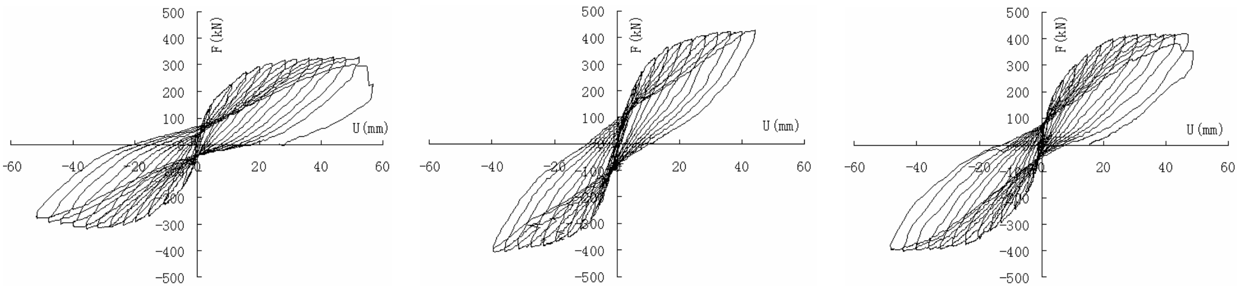

(a) TC1 (b) TC2 (c) TC3

Fig.5 Load-6displacement hysteretic response of specimens subjected to cyclic load

3.3. Bearing capacity and displacement

Table 1 shows cracking load, yield load, maximum load and ultimate load of specimens at all loading stages. Cracking load (F_{cr}) is the load when first crack was observed in testing and ultimate load (F_u) is the load when peak strength of the specimen dropped by approximately 15% of the maximum strength . F_y/F_u is yield ratio and U_u/ U_y is ductility coefficient.

Table 1.Load-carrying capacity and displacement

Specimen	axial Compression ratio	span-depth ratio	cracking load		yield load		maximum load		ultimate load		F_y/ F_u	U_u/ U_y
			F_{cr}	U_{cr}	F_y	U_y	F_d	U_d	F_u	U_u		
TC1	0.21	1.7	68.90	1.48	234.69	11.76	322.41	35.85	274.05	51.79	0.856	4.40
TC2	0.5	1.7	72.20	1.32	322.90	11.80	416.61	39.50	354.12	43.505	0.912	3.69
TC3	0.21	0.9	120.85	2.33	296.26	11.96	408.84	43.39	347.51	48.66	0.852	4.07

Cracking load and displacement of TC1 were similar to that of TC1 and didn’t increase when axial force increasing. It was because that the first crack occurred in the couple beams and couple beam’s behavior depended mainly on size and reinforcement ratio which were all same in TC1 and TC2. Cracking load of TC3 significantly increased of 75% than that of TC1, just due to increasing of span-depth ratio of coupling beam of TC3 which relatively improving the stiffness of coupling beam of TC3.

F_y, F_d and F_u of TC2 increased of 38%, 29% and 29% than that of TC1, showing the larger axial force improved the bearing capacity of core wall, evidently. Yield ratio of TC2 increased of 7% than that of TC1, indicating the core wall under larger axial force having a shorter process from yield load to ultimate load, which was a disadvantage to earthquake resistant. Cracking and yield displacement of TC2 were almost similar to that of TC1 but ultimate displacement of TC2 dropped of 15.9% than that of TC1, and ductility coefficient also dropped of 16.1%, indicating that deformability of core wall decreased significantly when axial compression ratio increased. F_y, F_d and F_u of TC3 increased of 26%, 27% and 27% than that of TC1, showing smaller span-depth ratio of coupling beam also could improved the bearing capacity of core wall, evidently. Ultimate displacement of TC3 dropped of 6% than that of TC1, and ductility coefficient also dropped of 7.5%, indicating that deformability of core wall also declined when span-depth ratio of coupling beam decreased.

3.4. Stiffness measured and stiffness attenuation coefficient

Table 2 shows stiffness measured and stiffness attenuation coefficient of specimens. K_0 is initial elastic stiffness, K_c is cracking stiffness, and K_y is yield stiffness. $\beta_{c0}= K_c/K_0$, $\beta_{yc}= K_y/K_c$, $\beta_{y0}= K_y/K_0$ are the stiffness attenuation coefficient of each specimen, respectively.

Table 2.Stiffness and coefficient of Stiffness degradation

Specimen	K_o/（kN·mm^{-1}）	K_c/（kN·mm^{-1}）	K_y/（kN·mm^{-1}）	β_{co}	β_{yc}	β_{yo}
TC1	50.91	46.55	19.96	0.914	0.429	0.392
TC2	55.46	54.70	27.36	0.986	0.5	0.493
TC3	62.43	51.87	24.77	0.831	0.476	0.397

K_y of TC2 obviously increased of 37 per than that of TC1, which was due to the larger axial force effectively restraining shear cracks and bending cracks from progressing, and restrictions on the deformation of whole specimen. β_{yo} of TC2 increased of 26 per than that of TC1, showing larger axial force made the stiffness attenuation slow down. K_0、K_c and K_y of TC3 increased of 23%, 11.4% and 24% than that of TC1, respectively. It likely due to the fact that increasing of span-depth ratio of coupling beams delayed the appearance and development of cracks in couple beams and made TC3 trend to behave as a whole structure. The stiffness attenuation coefficients of TC3 were similar to that of TC1, indicating increasing of span-depth ratio of coupling beams did little effect on stiffness attenuation amplitude at all loading stages.

3.5. Evaluation of the ductility

When specimens coming into the yield stage, the load increased slowly and didn’t reached the maximum quickly but the horizontal displacement significantly increased, so there was a long strengthen stage meaning good ductility. In this stage, bearing capacity improved evidently and the largest load-yield load ratio (F_u/F_y) was 1.37, 1.29 and 1.38.

When specimen TC1 reached the largest load, with displacement increasing, the bearing capacity declined slowly indicating good ductility. It was likely due to sufficient rotation of plastic hinge formed at the bottom of whole specimen and the ends of coupling beams and full development of bending and shears cracks under smaller axial compression ratio and coupling beam stiffness. When TC2 with bigger axial compression ratio and TC3 with more coupling beam stiffness reached the largest load, the bearing capacity declined rapidly and reached the ultimate bearing capacity very soon showing poor ductility.

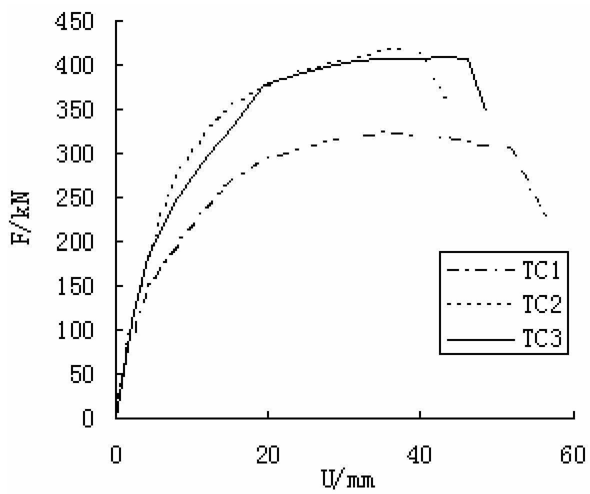

Fig 6.Envelopes of cyclic load-displacement curves

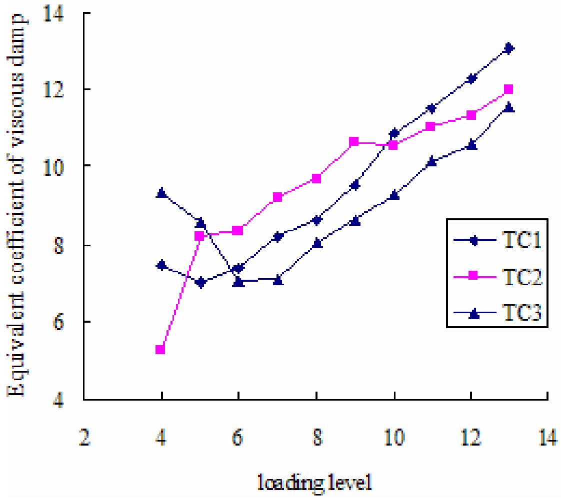

Fig 7.Equivalent coefficient of viscous damping curves

3.6. Energy dissipation by hysteretic behavior

Reinforced concrete core wall has two Stable ways to dissipate energy. The one is formation of plastic hinge at the bottom of the core wall and the other is formation of plastic hinge at the two ends of each coupling beam. The energy dissipated through hysteretic behavior can be measured as the area enclosed in the load-deformation curve when the structure undergoes repeated cycles of loading and this paper uses equivalent coefficient of viscous damping (HE) from the load-deformation curves to evaluate the energy dissipation of the core wall.

Figure 7 shows the equivalent coefficient of viscous damping- loading cycle level curve. Along with the formation of plastic hinge at the bottom of the core wall and at the ends of coupling beams and the development of a large amount of shear slip, the HE of each core wall was increasing stably indicating that the energy dissipated by specimens also increasing stably. Figure 7 indicates that HE of TC2 was most similar to that of TC1 and HE TC3 was obviously lower than that of TC1. It means that in this test, the axial compression ratio increasing from 0.2 to 0.5 didn't have much effect on energy dissipation but the span-depth ratio of coupling beam decreasing from 1.8 to 0.9 reduce the overall energy dissipation of specimens markedly.

3.7. Shear lag effect

In the flange wall of core wall, uniform strain doesn't exist and strain around corner posts is larger than average while strain far from corner post is less. In the web wall of core wall, strain distribution is also not linear. Those are called shear lag phenomenon. To study the shear lag effect of the reinforced concrete core wall, strain of vertical steels of the specimen were measured.

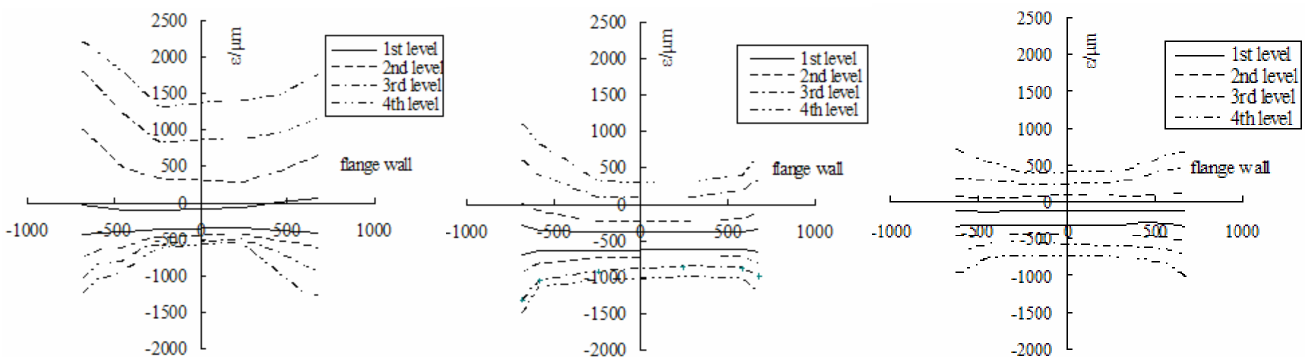

(a) TC1 (b) TC2 (c) TC3

Fig 8.Strain distributions on steel bars in the bottom of specimens

Figure 8 shows the strain distribution of the vertical steels at first floor along the flange wall when the cyclic lateral load at all levels achieve maximum. It can be seen that the strains of the vertical steels around the corner of each core wall are higher than that of the center and the shear lag effect is remarkable. With the load increases, shears lag effect increase obviously; The shear lag phenomenon of TC1 is even more significant than that of TC2 and the shear lag effect of TC3 is least among the specimens. It can be inferred that the higher axial compression ratio and span-depth ratio of coupling beam each can reduce the shear lag effect.

4. CONCLUSIONS

In this paper, three reinforced concrete core wall models with large height-width ratio, under the combined action of constant axial load and reversed cyclic lateral load, all had plastic hinges at the bottom of the core wall and the two ends of each coupling beam. After those plastic hinges rotating in full, specimens all were in overall bending damage in final. When the axial compression ratio increasing or span-depth ratio of coupling beam dropping, stiffness and load-carrying capacity of the specimen had risen markedly, but the ductility performance dropped significantly. In this test, the axial compression ratio increasing from 0.2 to 0.5 didn't have much effect on energy dissipation but the span-depth ratio of coupling beam decreasing from 1.8 to 0.9 reduce the overall energy dissipation of specimens markedly. In reinforced concrete core wall the shear lag effect is remarkable and the higher axial compression ratio and span-depth ratio of coupling beam each can reduce the shear lag effect.

REFERENCES

CAO Wan-lin, HUANG Xuan-ming, LU Zhi-cheng (2005). Experimental study on seismic behavior of reinforced concrete core walls with concealed bracings[J]. Earthquake Engineering and Engineering Vibration, 25(3):81-86.（in Chinese）

LU Xi-lin, LI Jun-lan (2002). Seismic behavior of reinforced concrete core walls subjected to cyclic loading[J]. Earthquake Engineering and Engineering Vibration, 22(3):45-50.（in Chinese）